Probing the Dynamic Interface between Trimethylamine Dehydrogenase (TMADH) and Electron Transferring Flavoprotein (ETF) in the TMADH−2ETF Complex: Role of the Arg-α237 (ETF) and Tyr-442 (TMADH) Residue Pair[†,‡]

Selena G. Burgess,[§,#] Hanan Latif Messiha,[⊥,#] Gergely Katona,[§] Stephen E. J. Rigby,[||] David Leys,[⊥] and Nigel S. Scrutton*[,⊥]

Department of Biochemistry, University of Leicester, Leicester LE1 9HN, U.K., School of Biological and Chemical Sciences, Queen Mary College, University of London, Mile End Road, London E1 4N5, U.K., and Manchester Interdisciplinary Biocenter, University of Manchester, 131 Princess Street, Manchester M1 7DN, U.K.

Received January 23, 2008; Revised Manuscript Received March 20, 2008

ABSTRACT: We have used multiple solution state techniques and crystallographic analysis to investigate the importance of a putative transient interaction formed between Arg-α237 in electron transferring flavoprotein (ETF) and Tyr-442 in trimethylamine dehydrogenase (TMADH) in complex assembly, electron transfer, and structural imprinting of ETF by TMADH. We have isolated four mutant forms of ETF altered in the identity of the residue at position 237 (αR237A, αR237K, αR237C, and αR237E) and with each form studied electron transfer from TMADH to ETF, investigated the reduction potentials of the bound ETF cofactor, and analyzed complex formation. We show that mutation of Arg-α237 substantially destabilizes the semiquinone couple of the bound FAD and impedes electron transfer from TMADH to ETF. Crystallographic structures of the mutant ETF proteins indicate that mutation does not perturb the overall structure of ETF, but leads to disruption of an electrostatic network at an ETF domain boundary that likely affects the dynamic properties of ETF in the crystal and in solution. We show that Arg-α237 is required for TMADH to structurally imprint the as-purified semiquinone form of wild-type ETF and that the ability of TMADH to facilitate this structural reorganization is lost following (i) redox cycling of ETF, or simple conversion to the oxidized form, and (ii) mutagenesis of Arg-α237. We discuss this result in light of recent apparent conflict in the literature relating to the structural imprinting of wild-type ETF. Our studies support a mechanism of electron transfer by conformational sampling as advanced from our previous analysis of the crystal structure of the TMADH−2ETF complex [Leys, D., Basran, J., Sutcliffe, M. J., and Scrutton, N. S. (2003) *Nature Struct. Biol. 10*, 219−225] and point to a key role for the Tyr-442 (TMADH) and Arg-α237 (ETF) residue pair in transiently stabilizing productive electron transfer configurations. Our work also points to the importance of Arg-α237 in controlling the thermodynamics of electron transfer, the dynamics of ETF, and the protection of reducing equivalents following disassembly of the TMADH−2ETF complex.

The electron transferring flavoproteins (ETFs[1]) are ubiquitous electron carriers that interact with structurally diverse redox partners (*1*). They mediate electron transfer between catabolic enzymes and membrane-bound electron acceptors, typically ETF-ubiquinone oxidoreductases (*1*). ETFs have important housekeeping functions in the oxidation of fatty acids and some amino acids, in both mammals and bacteria (*1, 2*). ETFs also have specialized roles in electron transfer under defined nutritional conditions, for example, in the oxidation of trimethylamine (*3*) and carnitine (*4, 5*), and in nitrogen fixation (*6*). All ETFs possess one equivalent of noncovalently bound FAD per ETF heterodimer, except the ETF from *Megasphaera elsdenii*, which contains 2 equivalents of FAD per dimer and one equivalent of AMP (*7*).

Methylophilus methylotrophus ETF is highly specialized and accepts electrons from the complex iron sulfur flavoprotein trimethylamine dehydrogenase (TMADH), which is required for the growth of *M. methylotrophus* on trimethylamine (*3, 8*). The complex formed by these two proteins has a highly dynamic protein−protein interface comprising the redox-active domain of ETF and the surface of TMADH (*9, 10*). This unusual interface is a consequence

[†] This work was funded by the UK Biotechnology and Biological Sciences Research Council. D.L. is a Royal Society University Research Fellow. N.S.S. is a BBSRC Professorial Research Fellow.

[‡] Atomic coordinates and structure factors (codes 3CLR, 3CLS, 3CLT, and 3CLU) have been deposited in the Protein Data Bank, Research Collaboratory for Structural Bioinformatics, Rutgers University, NJ (http://www.rcsb.org/).

* To whom correspondence should be addressed. Tel: +44 (0)161 306 5152. Fax: +44 (0)161 306 8918. E-mail: nigel.scrutton@manchester.ac.uk.

[§] University of Leicester.

[||] University of London.

[⊥] University of Manchester.

[#] These authors contributed equally to this work.

[1] Abbreviations: TMADH, trimethylamine dehydrogenase; ETF, electron transferring flavoprotein; EPR, electron paramagnetic resonance; ENDOR, electron−nuclear double resonance; ETF_{sq}, semiquinone form of ETF; ETF_{ox}, oxidized form of ETF; ETF_{hq}, hydroquinone form of ETF.

10.1021/bi800127d CCC: $40.75
Published on Web 04/12/2008

of the dynamic nature of ETF proteins in protein complexes (*9, 11*−*13*) and when free in solution (*14, 15*). The crystal structure of the TMADH−2ETF complex reveals a dual interaction mode at the protein−protein interface, a property that is also conserved in other ETF−primary dehydrogenase complexes (*11, 12*). Residue Leu β194 in *M. methylotrophus* ETF acts as an anchor and positions ETF onto a small hydrophobic patch located on the surface of TMADH. This interaction allows the highly flexible redox-active domain of ETF to sample local conformational space around the region of Tyr-442 (TMADH). Tyr-442 is known to facilitate rapid electron transfer to ETF (*16*), but owing to the lack of electron density for the FAD domain in the TMADH−2ETF complex, the precise role of Tyr-442 is unknown. One possibility is that it transiently arrests or suppresses FAD domain motion to facilitate rapid electron exchange from the 4Fe-4S center of TMADH to the FAD of ETF (*9*).

The lack of electron density for the FAD domain of ETF in the TMADH−2ETF complex has prevented detailed analysis of the protein−protein interface close to the point of electron transfer. Electron transfer is limited by biomolecular association of the partner proteins in the wild-type complex (*16*), but in mutant forms of TMADH (in which Tyr-442 is exchanged for alternative residues), electron transfer is limited by conformational reorganization within the complex (*16*). We infer that removal of a transiently stabilizing interaction[2] through mutagenesis of Tyr-442 would shorten the lifetime of the electron transfer competent conformation in which the tunnelling distance is <14 Å (*9*), thus impeding electron transfer in these mutant complexes. Residue Arg-α237 (ETF) is possibly involved in stabilizing the electron transfer competent conformation, although strong evidence for this role is lacking. Mutagenesis of Arg-α237 to Ala-α237 effectively abolishes electron transfer from TMADH to ETF (*17*), but the effects are multiple involving major changes in midpoint reduction potential of the FAD oxidized/semiquinone couple in ETF (*17*). It has so far not been possible to disentangle the combined effects of this mutation on the various aspects of the electron transfer mechanism (i.e., thermodynamics, rate of conformational sampling, stabilization of the reactive conformation, degree of electronic coupling, etc.). Deconvolving these different effects remain major challenges in the ETF field.

Compounding the problems associated with understanding the dynamics of the interface between TMADH and ETF is the issue of structural imprinting, a slow conformational change in ETF that is enabled by interaction with TMADH (*18*). These relatively slow structural changes associated with imprinting are not to be confused with conformational sampling. Unlike structural change imparted through the imprinting of ETF by interaction with TMADH, conformational sampling is an integral part of the electron transfer mechanism (*9*).

[2] The precise nature of the interaction is unclear in the absence of electron density for domain II in the TMADH−2ETF complex, and in principle, it could be a conventional H bond between Tyr-442 (TMADH) and Arg-α237 (ETF) (i.e., a head-to-head interaction) or a cation-π interaction (with the arginine side chain stacking over the edge of the phenolic side chain of Tyr-442). Our modeling (*9*) implies the former is more likely. Also, note in the related electron transfer complex formed between human medium chain acyl CoA dehydrogenase and ETF, a glutamate residue (instead of tyrosine) forms a transient interaction with the arginine residue in ETF.

The redox properties of *M. methylotrophus* ETF are distinct from those of other ETFs. The FAD reduction potential of the oxidized/semiquinone couple in wild-type ETF (E'_1) is +153 ± 2 mV, which indicates exceptional stabilization of the flavin anionic semiquinone species (*17*). Conversion to the dihydroquinone is incomplete ($E'_2 < -250$ mV), consistent with the presence of a kinetic block on full reduction of the FAD, but this kinetic block is relieved in the TMADH−2ETF complex (*19*), suggesting structural differences between bound and free forms of ETF. The structure of ETF indicates that Arg-α237 is located over the *si* face of the FAD isoalloxazine ring (*9*) and that in this position it contributes to the exceptional stabilization of the FAD_{sq}. Mutagenesis (Arg-α237 to Ala-α237) leads to a substantial destabilization of the FAD_{sq} by ~200 mV (*17*).

Herein, we have investigated further the role played by Arg-α237 in complex assembly, electron transfer, and imprinting of ETF through the isolation and study of several mutant ETFs. Through multiple solution state techniques and crystallography, we show that the rate of electron transfer is substantially slowed on mutating this residue. We demonstrate that Arg-α237 is important for poising the reduction potential of the ETF FAD to facilitate electron transfer from TMADH and for the protection of reducing equivalents in ETF. We also show that structural imprinting of ETF requires Arg-α237, and we clarify some of the controversies that have arisen regarding the phenomenon of imprinting in *M. methylotrophus* ETF. Our studies provide a deeper understanding of electron transfer in this complex system and point to key and multiple roles for Tyr-442 (TMADH) and Arg-α237 (ETF) in the conformational sampling mechanism of electron transfer in the TMADH−2ETF complex.

EXPERIMENTAL PROCEDURES

Mutagenesis and Purification of ETF. The mutant ETF proteins (αR237K, αR237E, and αR237C) were isolated using the Stratagene Quikchange mutagenesis protocol using plasmid pED1 as the template (*14*). To ensure that no spurious changes had arisen as a result of the mutagenesis reaction, the entire ETF gene was resequenced. The isolation of mutant αR237A has been described previously (*17*). A fifth mutant form (αR237Y) was isolated at the DNA level, but we were unable to express functional ETF protein from this construct. Expression of wild-type and mutant recombinant proteins was performed in *E. coli* strain JM109. The exception was mutant αR237E, which was expressed in *E. coli* strain XL1 Blue. Recombinant strains were grown in LB medium containing 100 μg/mL ampicillin to an optical density of ~0.5 at 600 nm, and protein expression was induced by the addition IPTG (0.05 mM for mutant αR237C and 0.01 mM for the wild-type and the remaining mutant proteins). Following the addition of IPTG, cultures were grown for a further 12 h. Cells were resuspended in 20 mM potassium phosphate buffer, pH 7.2 (buffer A), and lysed using a French Press. DNA was degraded by the addition of deoxyribonuclease (10 μg/mL broken cells) and 20 mM magnesium chloride for 30 min. Cellular debris was removed by centrifugation and the supernatant fractionated by the addition of ammonium sulfate to 50% saturation. Following centrifugation, the supernatant was applied to a Phenyl Sepharose HP XK26 column equilibrated with 20 mM

potassium phosphate, pH 7.2, containing 1.5 M ammonium sulfate and 0.2 mM EDTA (buffer B), and eluted using a descending gradient (1.5 to 0 M ammonium sulfate). Fractions containing ETF protein were dialyzed exhaustively against buffer A. Fractions were subsequently applied to a Q-Sepharose HP XK26 column equilibrated with buffer A and eluted using an ascending gradient (0 to 2 M) of potassium chloride contained in buffer A. Fractions containing protein were either dialyzed exhaustively against buffer A or desalted using Sephadex G25 prior to storage at −80 °C in the presence of 20% ethylene glycol. The concentration of ETF solutions was calculated using an extinction coefficient of 11,300 M^{-1} cm^{-1} (*3*) for the oxidized protein at 438 nm (wild-type) or 450 nm (mutant proteins). The absorbance spectrum of wild-type and some of the mutant proteins indicated they were purified as a mixture of the oxidized and semiquinone forms. Thus, for some of the reported studies, prior to analysis, these protein samples were oxidized with potassium ferricyanide. Samples were then purified further using a Biorad 10 DG column.

Mutagenesis and Protein Purification of TMADH. Native TMADH from *M. methylotrophus* (sp. W_3A_1) was purified as described previously (*20*). His-tagged TMADH was constructed by inserting six histidine residues at the C-terminus of recombinant TMADH using the Quikchange Site-directed Mutagenesis Kit procedure from Stratagene. Recombinant TMADH and His-tagged TMADH were purified as described previously (*21*). The concentration of native TMADH was calculated using the molar extinction coefficient (ϵ_{443} = 27,300 M^{-1} cm^{-1}) for the oxidized enzyme (*20*). The recombinant native and the His-tagged TMADH enzymes contained the full complement of the 4Fe-4S center and ADP, but the level of flavinylation is ∼30% that of native TMADH. Partial flavinylation is known not to affect the kinetic behavior of the enzyme dimer (*21*); the structure of the TMADH−2ETF complex indicates that the docking site on the surface of TMADH for ETF (i.e., the site for molecular imprinting; see results) is distant from the active site that contains the 6-*S*-cysteinyl FMN. The concentration of recombinant TMADH enzymes was measured using the extinction coefficient (ϵ_{280} = 201,610 M^{-1} cm^{-1}) for the oxidized (as purified) protein at 280 nm, determined as described previously (*22*).

Reduction of ETF Proteins. Reduction of oxidized ETF with sodium dithionite was performed anaerobically at 25 °C in 50 mM potassium phosphate at pH 7.0 inside a Belle Technology glovebox (<2.0 ppm oxygen). The concentration of dithionite was calculated by titration against 1 mM FAD. Reduction of oxidized ETF enzymes by catalytic amounts of TMA-reduced TMADH was also performed anaerobically at 25 °C in 50 mM potassium phosphate at pH 7.0 inside the glovebox. The reaction mixture contained 26 μM oxidized ETF, 0.1 μM TMADH (or 1 μM TMADH for reactions with the αR237C ETF), and 10 mM TMA. Spectral changes reporting on reduction of ETF were recorded using a Jasco V530 spectrophotometer.

Steady-State Kinetic Assays. Steady-state kinetic assays of ETF reduction by TMADH were performed aerobically at 25 °C using a Cary 50 Bio spectrophotometer. ETF was oxidized prior to assay via treatment with potassium ferricyanide followed by gel filtration (BioRad 10DG). The reaction mixture contained 50 mM potassium phosphate buffer, pH 7.0, and a fixed concentration of native TMADH; various ETF concentrations were added, and the reaction was initiated by the addition of TMA (100 μM). The initial velocity of the reaction (v_i) was obtained by measuring the rate of the reaction at the peak of flavin absorbance (450 nm) and reaction rates calculated using a difference extinction coefficient between oxidized and semiquinone ETF [$\Delta\epsilon_{450}$ = 7,830 M^{-1} cm^{-1} (*3*)]. The Michaelis−Menten equation was used to fit data in plots of reaction rate versus ETF concentration.

Redox Potentiometry. Redox titrations were performed at 25 ± 2 °C in 50 mM potassium phosphate buffer, pH 7.0, in a Belle Technology glovebox under anaerobic conditions (oxygen maintained at <5 ppm). Enzyme solutions (60 − 70 μM in ∼10 mL of titration buffer) were electrochemically titrated according to the method of Dutton (*23*) using sodium dithionite as reductant and potassium ferricyanide as oxidant. Mediators were added to facilitate electrical communication between the enzyme and the electrode prior to titration. Typically, 5 μM 2-hydroxy-1,4-napthaquinone, 2 μM phenazine methosulfate, 1 μM methyl viologen, and 1 μM benzyl viologen were included in the titration as redox mediators for the titrations. The electrochemical potential of the enzyme solutions was measured using a combination pH/voltmeter coupled to a platinum/calomel electrode (ThermoRussell Ltd.) that had been previously calibrated using the Fe^{3+}/Fe^{2+} EDTA couple (+108 mV). The observed potentials were corrected by +244 mV relative to those for the standard hydrogen electrode (SHE) (Pt/calomel + 244 mV). The electrode was allowed to stabilize between each addition of reductant or oxidant, and spectra (300−700 nm) were recorded using a Cary 50 UV−visible scanning spectrophotometer (Varian) via a fiber optic cable immersed in the enzyme solution and connected to the external spectrophotometer. The spectra of at least 30 to 40 points across a whole range of redox potentials during the process of reduction and oxidation were recorded. Titrations were performed over a 5 to 7 h period. Equilibration was achieved throughout the titrations, and no hysteretic behavior was observed. For the αR237E and αR237C ETF proteins, plots of the absorbance values of 470 nm (near the oxidized flavin maximum) and 370 nm (close to the maximum of the anionic semiquinone) against redox potential were fitted to eq 1, which represents a 2-electron redox process derived by extension of the Nernst equation and the Beer−Lambert law as described previously (*17, 23*):

$$A = \frac{a10^{(E-E_1')/59} + b + c10^{(E_2'-E)/59}}{1 + 10^{(E-E_1')/59} + 10^{(E_2'-E)/59}} \quad (1)$$

In equation 1, A is the absorbance value (at either 470 nm or at 370 nm) at the electrode potential E, and a, b, and c are the component absorbance values of the fully oxidized, semiquinone, and reduced states, respectively. E_1' and E_2' are the midpoint potential for oxidized/semiquinone and semiquinone/reduced couples, respectively. Spectral changes for the αR237K ETF were analyzed as described for wild-type and αR237A ETFs (*17*). Data manipulation and analysis were performed using the Grafit software package version 5.0. All redox potentials are given relative to the standard hydrogen electrode.

Structural Imprinting of ETF by TMADH. Structural imprinting reactions (*18*) were carried out aerobically and

Table 1: Data Collection and Refinement Statistics for αR237K, αR237C, αR237E, and αR237A ETF Structure Determination

	αR237K ETF	αR237C ETF	αR237E ETF	αR237A ETF
		data set		
space group	$P6_1$	$P6_1$	$P6_1$	$P6_1$
resolution (Å)	19.0 − 1.8	20.0 − 1.65	20.0 − 2.0	20.0 − 1.9
unique reflections	58203	72327	41782	49299
completeness (%)	99	95.6	99.9	99.8
R_{sym} (%)[a]	0.067	0.084	0.062	0.074
$I/\sigma I$	9.2	7.3	11.2	8.6
redundancy	4.2	3.8	4.5	5.8
		refinement		
resolution (Å)	19.0 − 1.8	20.0 − 1.65	20.0 − 2.0	20.0 − 1.9
R factor (%)[b]	17.0	16.5	15.5	15.0
R_{free}[b]	20.4	19.1	18.6	18.2
rms deviations				
bond length (Å)	0.013	0.019	0.009	0.014
bond angles (°)	1.54	1.84	1.30	1.56

[a] $R_{sym}(I) = \Sigma_h\Sigma_i|I_{h,i} - \langle I_h\rangle|/\Sigma_h\Sigma_i I_{h,i}$, where I is the observed intensity, $\langle I\rangle$ is the average intensity of multiple observations of symmetry related reflections. [b] $R_{cryst} = \Sigma||F_o| - |F_c||/\Sigma|F_o|$, R_{free} is the same as R_{cryst} but was calculated using a separate validation set of 5% of the reflections that were excluded from the refinement process.

anaerobically at 25 °C in 50 mM potassium phosphate buffer at pH 7.0. Fluorescence and absorption spectra of ETF were followed during the reaction. The imprinting reactions were initiated by the addition of 5 μM TMADH (native, recombinant, or His-tagged TMADH) to 50 μM ETF [complex dissociation constant ∼10 μM (*19*)]. For fluorescence analysis, static fluorescence spectra were measured using a Cary Eclipse fluorescence spectrophotometer. Emission spectra were collected from 460 to 700 nm, exciting at 450 nm. Imprinting of ETF by TMADH was followed by plotting the emission at 540 nm at regular time intervals. A control containing only ETF was run in parallel. For spectrophotometric analyses, absorbance spectra were also recorded between 200 and 700 nm using a Jasco V-530 spectrophotometer.

To investigate the reversibility of the imprinting reaction of wild-type ETF by TMADH, the as-purified ETF (50 μM) was incubated with His-tagged TMADH (5 μM) until no further increase in fluorescence was observed (6.5 h). His-tagged TMADH was then removed from the reaction mixture by adsorption on Ni-Sepharose resin that had been previously equilibrated with 50 mM potassium phosphate buffer at pH 7.0. The resin was added to the reaction in 3 aliquots of 200 μL volume each. Following the addition of each aliquot of resin, the reaction mixture was mixed with the resin then centrifuged at 15,000 rpm at 20 °C. The fluorescence of ETF, as well as the absorption spectrum of the protein, was determined after removing the His-Tagged TMADH from the reaction.

Analysis of Structural Change by EPR Spectroscopy. Structural changes in wild-type ETF (semiquinone form at a concentration of 50 μM) following incubation with TMADH (4.5 μM oxidized protein) were monitored by analysis of flavin fluorescence emission as a function of time and by EPR spectroscopy. EPR spectroscopy was undertaken on 300 μL samples of semiquinone ETF (50 μM) contained in 50 mM potassium phosphate at pH 7.0 at 25 °C. Wild-type ETF (unimprinted; purified predominantly in the semiquinone state) and imprinted wild-type ETF were placed directly into standard 3 mm quartz EPR tubes and frozen in liquid nitrogen. For mutant ETFs, oxidized proteins were reduced anaerobically to the semiquinone state using a FAD-calibrated sodium dithionite solution prior to sample storage in liquid nitrogen. EPR samples of ETF_{sq} were also prepared by the addition of the paramagnetic complex, Co^{2+}:EDTA. The complex to ETF_{sq} molar ratio was 5:1. The paramagnetic complex was generated as a 2:1 molar mixture of $CoCl_2 \cdot 6H_2O$ and EDTA, respectively. EPR spectra were collected at 70 K on a Bruker ELEXSYS E500 spectrometer with an Oxford Instruments ESR900 liquid helium cryostat. Each EPR spectrum recorded was the average of two scans. Spectra were measured for each sample following the application of 10, 20, 50, 100, and 200 μW. The integral of each EPR spectrum was calculated using Xepr software (Bruker). Spectral readings were normalized to the same integral value at 10 μW to allow comparison between different samples.

Crystallography. Prior to crystallogenesis, ETF mutants were subjected to limited proteolysis using 0.1 mg/mL trypsin for 4 h at room temperature to remove a portion of the recognition peptide in ETF and thus aid crystallogenesis (*9*). Proteolysis was terminated by the addition of 0.1 mg/mL trypsin 1inhibitor. Crystallization was performed as described previously (*9*). Crystals were flash-cooled in oil and stored in liquid nitrogen. Data sets were collected at ESRF (Grenoble, France) and processed and scaled with the HKL programs, DENZO, and SCALEPACK (*24*). Structure determination was carried out using the structure for wild-type *M. methylotrophus* ETF [PDB code 1O97; (*9*)] as a starting model, refined against the respective mutant data sets using Refmac (*25*). The models were systematically improved through iterative cycles of TLS refinement and manual rebuilding. The structure of the R237C βETF mutant was the only exception where TLS refinement was not used because of the instability of the TLS parameters. The models were checked by cross validated SigmaA weighted electron density maps calculated with both $2mF_o - DF_c$ and $mF_o - DF_c$ coefficients (*25*). The solvent was rebuilt in each case using the Arp/wArp suite (*26*). A random selection of approximately 5% of the data (test set) was assigned for calculation of the free *R* factor and was not included in the refinement. The refinement statistics are summarized in Table 1. Structure factors and associated coordinates are deposited with the Protein Data Base.

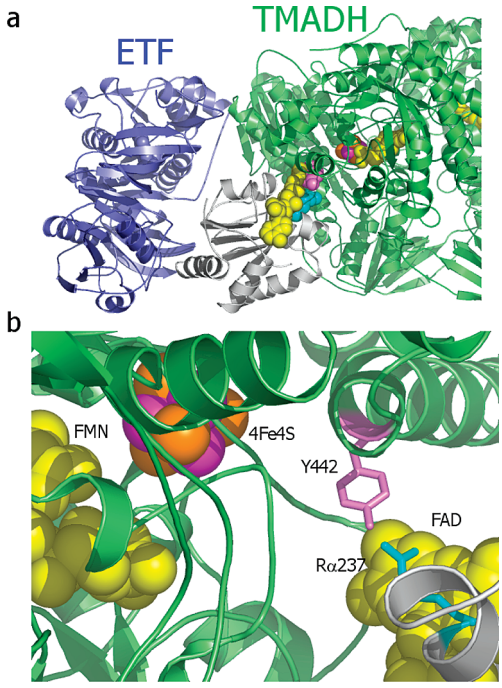

FIGURE 1: Structure of the TMADH−2ETF electron transfer complex. Panel a: Ribbon representation illustrating one subunit of TMADH (depicted in green) in complex with ETF. Domains I and III of ETF are shown depicted in blue ribbons; domain II is not defined in crystallographic studies [i.e., there is no observable electron density (*9*)]. Domain II is shown modeled in grey ribbons in a putative electron transfer competent conformation identified from weighted masses molecular dynamics simulations (*9*). The flavin cofactors in TMADH and ETF are shown in yellow space fill mode and the 4Fe-4S center (TMADH) in brown/purple. Residue Tyr-442 (TMADH) is shown in purple and Arg-α237 (ETF) in blue. Panel b: Detail of the putative interaction between Tyr-442 (TMADH) and Arg-α237 (ETF) in the proposed electron transfer competent geometry shown in panel a. Colors are as defined in panel a.

RESULTS

Potential Role of Arg-a237 (ETF) and Tyr-442 (TMADH) in Complex Assembly and Electron Transfer. The crystal structure of the TMADH−2ETF complex reveals a dual interaction interface in which (i) domain III of ETF (the anchor domain) interacts with TMADH through a recognition peptide sequence, and (ii) the redox-active FAD binding domain (domain II) samples conformational space to search out optimum geometries for electron transfer (*9*) (Figure 1). Weighted masses molecular dynamics simulations of the conformational sampling of reactive configurations suggest that, in those geometries where electron transfer is possible, Arg-α237 (ETF) is located close to Tyr-442 (TMADH) (*9*). We have suggested previously that transient interaction of these residues might increase the lifetime of the electron transfer competent state and thus facilitate catalysis in the TMADH−2ETF complex (*9*). We have probed the mechanism of electron transfer in TMADH−2ETF complexes in which Tyr-442 has been targeted by mutagenesis. In the wild-type complex, electron transfer is limited by bimolecular association of the partner proteins, whereas in the mutant complexes, conformational events after initial docking of the proteins are suggested to limit the electron transfer rate (*16*). We hypothesize that capture of the electron transfer competent state is impeded in the mutant complexes owing to the removal of one part of the hook (Tyr-442) required for transient stabilization of electron transfer competent state (s). This is consistent with targeted cross-linking data between these residue positions in mutants where Arg-α237 and Tyr-442 have been replaced by cysteine residues (*9*).

Although we have reported the properties of an αR237A ETF mutant in relation to control of the reduction potential of the ETF cofactor FAD (*17*), to date there has been no systematic report of the properties of mutant ETFs altered in this region in relation to residue type at position α237 and the effects of mutations on (i) the kinetics and thermodynamics of electron transfer, (ii) ETF structure, and (iii) conformational properties of ETF. With this in mind and to obtain deeper insight into the mechanism of electron transfer linked to conformational sampling (*9*), we have studied the properties of four mutant ETFs (αR237K, αR237A, αR237C, and αR237E). A complicating issue is the phenomenon of structural imprinting of wild-type ETF by TMADH (*18*) and the relevance (if any) this might have to biological function. Our initial studies (reported below) therefore set out to clarify aspects of the imprinting phenomenon prior to a detailed analysis of the αR237 mutant ETF proteins.

Structural Imprinting of ETF_{sq} by TMADH Is Essentially Irreversible in Vitro and Is Prevented by Redox Cycling. ETF as purified from *M. methylotrophus* or *E. coli* is obtained as a mixture of oxidized ETF and semiquinone ETF, but the predominant form (>80%) is the semiquinone species. This as-purified form of ETF isolated from the native host *M. methylotrophus* or recombinant strains of *E. coli* is structurally altered, or imprinted, during prolonged incubation with TMADH (*18*). This conformational change is accompanied by a significant change in the ETF flavin fluorescence, which has been attributed to confined reorganizations within the vicinity of the protein-bound FAD (*18*). Our previous study was not able to deconvolve the contribution made by (i) ETF in complex with TMADH and (ii) free ETF to these fluorescence changes. We have now achieved this by isolating a C-terminal His-tagged version of TMADH that enables rapid removal of TMADH from ETF following the imprinting reaction. Incubation of the as-purified wild-type ETF with native TMADH (from *M. methylotrophus*), recombinant TMADH (from *E. coli*) or His-tagged TMADH (from *E. coli*) resulted in fluorescence and optical spectral changes of the ETF-bound FAD. The intensity of the FAD fluorescence emission of ETF was increased by ∼360%, 350%, and 380% of the original fluorescence intensity following incubation with native TMADH, recombinant TMADH, and His-tagged TMADH, respectively (Figure 2A−C). These increases in fluorescence were recorded up to the stage where no further change in fluorescence emission was observed. Prolonged incubation was required to achieve the full fluorescence change (∼7 h with native TMADH; ∼9 h with recombinant TMADH; ∼6.5 h with His-tagged TMADH), consistent with our previous report with native TMADH (*18*). Control experiments in which the fluorescence of ETF was monitored in the absence of TMADH demonstrated that ETF does not develop significant enhanced fluorescence over a 9 h period compared to samples incubated with TMADH. Significant and similar changes in the UV−visible spectrum of ETF were observed during imprinting by TMADH (native, recombinant or His-tagged; Figure 2D). The ETF spectrum after imprinting with

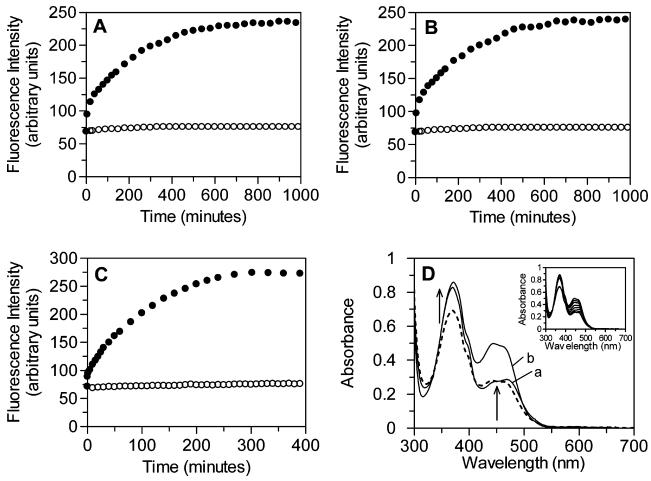

FIGURE 2: Fluorescence and absorbance changes following incubation of as-purified wild-type ETF with TMADH. Panel A: Time dependence of induced emission (540 nm) following excitation (450 nm) of the as-purified wild-type ETF upon incubation with native TMADH (●). The fluorescence of as-purified ETF as a function of time in the absence of TMADH is shown as open circles (○). Panel B: Same as that for panel A, except recombinant TMADH replaces native TMADH. Panel C: Same as that for panel A, except His tagged recombinant TMADH replaces native TMADH. Panel D: Main panel, absorbance changes of the as-purified ETF observed during incubation with native TMADH. The spectra were obtained by subtracting the TMADH spectrum from the acquired spectra to yield spectra of imprinted ETF at time intervals. Dashed line, spectrum of as-purified ETF; spectrum a, ETF spectrum after 2 min of imprinting with TMADH; spectrum b, ETF spectrum after 7 h of imprinting. Inset, the change in ETF spectrum during imprinting (spectra were collected over 7 h during the imprinting reaction). The spectra shown are those with the TMADH contribution subtracted. Conditions: as-purified wild-type ETF (50 μM) and TMADH (5 μM) in 50 mM potassium phosphate buffer at pH 7.0 at 25 °C.

TMADH has FAD semiquinone signature, suggesting that imprinting is not related to release of FAD from the protein. Similar absorbance changes were not obtained for ETF samples incubated in the absence of TMADH. UV−visible and fluorescence changes indicative of imprinting were observed under aerobic and strictly anaerobic conditions, indicating that imprinting is not related to reoxidation of the flavin.

To investigate any reversibility of the imprinting reaction of wild-type ETF by TMADH, the as-purified ETF was incubated with His-tagged TMADH for 6.5 h (until no further increase in fluorescence was obtained). His-tagged TMADH was then removed from the reaction mixture by adsorption on Ni-Sepharose resin, and both the fluorescence and UV−visible spectrum of imprinted ETF were determined. The fluorescence of ETF remained similar to that developed after full imprinting and within 16 h did not relax back to its original form, suggesting that the observed fluorescence and spectral changes are essentially irreversible. After removing His-tagged TMADH, the UV−visible spectrum of ETF is similar to the ETF spectrum obtained after full imprinting but in the presence of TMADH. (Note: the spectrum of ETF in ETF/TMADH mixtures was obtained by subtracting the TMADH spectrum from the combined ETF/TMADH spectrum.) This emphasizes the essentially irreversible nature of the structural change in ETF following interaction with TMADH. The altered nature of the FAD spectrum in imprinted ETF is not attributed to FAD

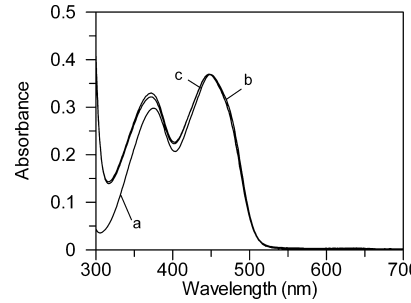

FIGURE 3: Spectra of released flavin obtained after treating both the as-purified and the imprinted forms of wild-type ETF with proteinase K. Spectrum a, commercial FAD treated in the same way as the ETF samples. Spectrum b, FAD released from as-purified ETF. Spectrum c, FAD released from imprinted ETF. For spectrum c, as-purified wild-type ETF (50 μM) and His-tagged TMADH (5 μM) were incubated in 50 mM potassium phosphate buffer at pH 7.0 for 6.5 h. His tagged TMADH was removed as described in Experimental Procedures. ETF samples (as purified and imprinted forms) were incubated for 4 h at 40 °C with proteinase K prior to analysis.

modification as shown by incubating as-purified ETF and imprinted ETF with proteinase K to release FAD and analysis of the liberated cofactor spectrum (Figure 3). Also, the mass of the recovered cofactor was that of FAD for both samples.

The fluorescence emission intensity of oxidized ETF (ETF_{ox}; generated by treatment with potassium ferricyanide) is ~20% that of as-purified ETF. When incubated with TMADH, the fluorescence emission of ETF_{ox} did not increase, suggesting that the ETF_{ox} does not imprint (Figure S1A). Also, the UV−visible spectrum of ETF_{ox} was not perturbed appreciably on addition of TMADH (Figure S1B). ETF_{sq} can be generated by oxidizing the as-purified protein with potassium ferricyanide, followed by reductive titration with sodium dithionite. For ETF_{sq} produced in this way, we were unable to demonstrate any imprinting behavior on incubating with TMADH (Figure S1C). This suggests that ETF_{sq} generated chemically through redox cycling differs in structure compared with as-purified ETF (which is predominantly in the semiquinone form). Titration by dithionite can convert as-purified ETF to the ETF_{sq} in which all of the FAD is reduced to the semiquinone level. ETF_{sq} generated in this way has a different UV−visible spectrum compared to as-purified ETF, reflecting conversion of the small amount of ETF_{ox} (<20%) in the as-purified ETF sample to ETF_{sq}. Following the removal of excess dithionite from this sample by rapid gel filtration, we found it was possible to imprint this reduced form of ETF in a manner similar to that for the as-purified form of ETF (Figure S1D). This suggests that treatment with dithionite alone does not affect the imprinting properties of the semiquinone form of ETF in the original as-purified sample. We infer that redox cycling (i.e., conversion to the oxidized form with ferricyanide followed by reduction with dithionite) is required to prevent the imprinting reaction.

EPR Spectroscopy of ETF. Saturation EPR signal profiles for as-purified and fully imprinted ETF were obtained by measuring EPR spectra of the proteins as a function of increasing microwave power. The integral of each spectrum was calculated and to enable comparison between different samples the integrals were normalized to the value obtained at 10 μW. As-purified ETF was found to saturate more readily than imprinted ETF. This is consistent with the FAD

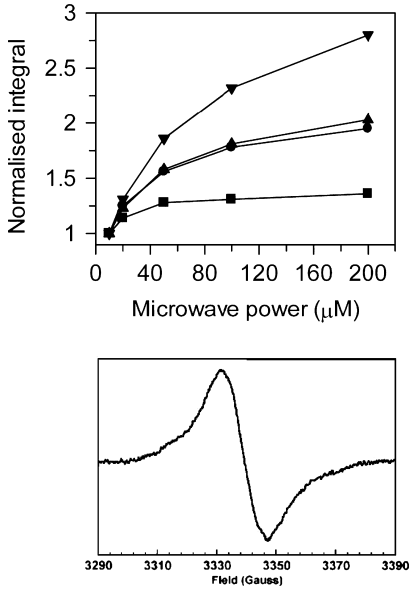

FIGURE 4: Upper panel: EPR microwave energy saturation profiles obtained for wild-type ETF proteins in the FAD semiquinone redox state for both the as-purified and imprinted forms of wild-type ETF. ■, saturation plot of as-purified ETF; ●, saturation plot of as-purified ETF in the presence Co^{2+} ions; ▲, saturation plot of imprinted ETF; ▼, saturation plot of imprinted ETF in the presence Co^{2+} ions. Conditions: semiquinone ETF was contained in 50 mM potassium phosphate at pH 7.0. EPR spectra were acquired at 70 K. Lower panel: typical ETF EPR spectrum (wild type shown) recorded using 10 μW microwave power and 1.2 G modulation amplitude at 70 K; two scans were co-added.

in the imprinted ETF being held in a more flexible environment (Figure 4). Increased flexibility in the flavin environment aids relaxation of the excited electron through energy loss attributed to molecular vibrations. The effect of adding Co^{2+} on the saturation properties of as-purified and imprinted ETF is also consistent with this notion. Interactions between Co^{2+} and the excited flavin cofactor are expected to reduce the saturation effect observed for the wild-type protein. This interaction is dependent on the relative exposure of the flavin to the solvent, and thus the Co^{2+} ion. Saturation was decreased on adding Co^{2+} to as-purified and imprinted ETF, consistent with the flavin being exposed to bulk solvent in each form of ETF (Figure 4). However, saturation was relieved to a greater extent on adding Co^{2+} to imprinted ETF compared with the as-purified ETF sample, suggesting that the flavin semiquinone is relatively more exposed to the bulk solvent in the imprinted form of ETF.

Our data suggest that the interaction of TMADH with ETF_{sq} alters the FAD environment. The likely origin of this structural change is in the nature of the contact of domain II of ETF (the mobile FAD domain; Figure 1) with the surface of TMADH. The crystal structure of the TMADH−2ETF complex and the results of our modeling analyses suggest that an interaction between αArg-237 (ETF) and Tyr-442 (TMADH) is potentially the main interaction at this protein interface (*9*). For this reason, we have isolated a series of mutants at position αArg-237 to probe the importance of this potential interaction in the electron transfer complex and structural imprinting.

Properties of Mutant TMADH−2ETF Complexes Suggest Arg-α237 Is a Key Interacting Residue at the Dynamic Protein Interface between TMADH and ETF. The αR237K, αR237E, αR237C, and αR237A ETF proteins were purified

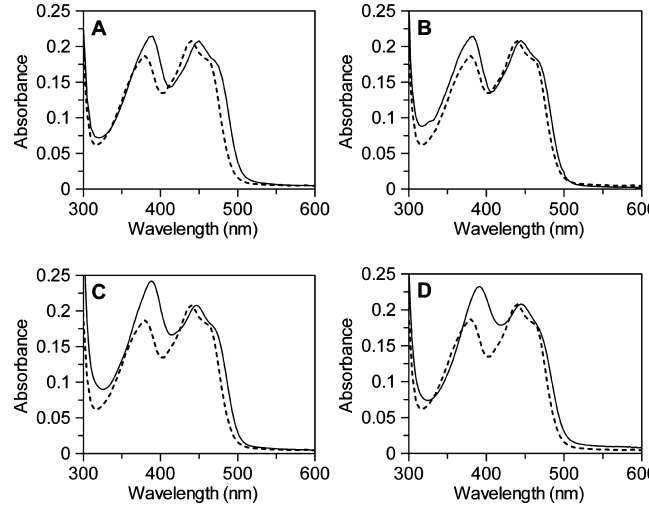

FIGURE 5: UV−visible spectra for the oxidized forms of the mutant ETF proteins. The dashed line in all panels is the spectrum of oxidized wild-type ETF with spectral maxima at 380 and 438 nm, and A_{380}/A_{438} of 0.9. Panel A: spectrum (solid line) of oxidized αR237K ETF with spectral maxima at 390 and 450 nm, and a ratio of absorbance at 390 nm versus 450 nm (A_{390}/A_{450}) of 1.03. Panel B: spectrum (solid line) of oxidized αR237C ETF with spectral maxima at 382 and 444 nm, and A_{382}/A_{444} of 1.01. Panel C: spectrum of oxidized αR237E ETF with spectral maxima at 388 and 448 nm, and A_{388}/A_{448} of 1.16. Panel D: spectrum of oxidized αR237A ETF with spectral maxima at 388 and 446 nm, and A_{388}/A_{446} of 1.01. All ETF proteins were contained in 50 mM potassium phosphate at pH 7.0.

as described above. As for wild-type ETF, αR237K ETF was generated as a mixture of the oxidized and semiquinone protein, with the semiquinone predominating. The remaining ETF mutants were produced in the oxidized state. In the oxidized state, compared with wild-type ETF_{ox}, the wavelength maxima of the flavin peaks in the mutant proteins were all shifted to longer wavelength (Figure 5), suggesting that the FAD is relatively more solvent exposed in the mutant proteins. Also, the absorbance peak at ~370 nm is relatively more intense than the peak at ~450 nm for the mutant proteins compared with wild-type, and in the case of the αR237A, the shoulder on the ~450 peak is absent (Figure 5D). Combined, the data suggest a more hydrophobic environment for the FAD isoalloxazine ring in wild-type ETF compared with that for the mutant ETFs. This is consistent with the location of Arg-α237 in the crystal structure of wild-type ETF, which shields the *si*-face of the FAD (*9*).

Difference spectra produced from UV−visible absorption changes observed for oxidized wild-type ETF and the αR237A mutant on binding TMADH have been published (*17, 19*) and indicate perturbation of the environment of the FAD cofactor in ETF. Difference spectra produced for oxidized αR237K, αR237C, and αR237E ETF on binding oxidized TMADH (Figure S2) identified the spectral changes accompanying complex formation. These difference spectra obtained vary from those seen for the wild-type complex. Also, unlike for the wild-type complex, the difference spectral changes for the mutant complexes were not complete within the mixing time. This indicates that the kinetics of formation of the final equilibrium state for the oxidized TMADH−2ETF complexes are substantially perturbed on mutating Arg-α237. The difference spectra accompanying the formation of the oxidized TMADH−2ETF(αR237C) and TMADH−2ETF(αR237E) complexes are similar and com-

plete within ~2 h (Figures S2B and S2D, respectively). The spectral changes accompanying the formation of the oxidized TMADH−2ETF(αR237A) (*17*) and TMADH−2ETFαR237K) (Figure S2A) complexes differed from those complexes formed with αR237C and αR237E ETFs, suggesting an altered geometry in the assembled complex. Complex formation was most protracted with the TMADH−2ETF(αR237A) complex with the difference spectral changes taking ~5 h to develop (*17*). The slower kinetics of formation of the equilibrium mutant complexes and the perturbed spectral changes on forming the mutant complexes implicate residue Arg-α237 as a key interacting residue at the dynamic protein interface of the TMADH−2ETF complex. We wish to emphasize that the very slow spectral changes are unlikely the result of slow electron transfer between the partner proteins. Both proteins were treated with ferricyanide prior to binding studies to ensure that they were fully oxidized. Although the precise nature of the very slow conformational events that give rise to the spectral changes are at this stage unclear, the data illustrate that complex formation occurs following mutation of Arg-α237. As the structure of the mutant ETFs are essentially identical with wild type ETF (with the obvious change in residue position; see below) we assume that (i) contact with the anchor domain (domain III) is not impaired as this is located far from the point of mutation in a separate domain of ETF (*9*) and that (ii) the observed spectral changes reflect small conformational adjustments of the redox-active FAD-binding domain of ETF (domain II) as a result of interaction with TMADH. The origin of these spectral changes will require more detailed analyses and are beyond the scope of this current article, and it is suffice to state that they demonstrate an interaction between TMADH and ETF followed by slow structural readjustments that contribute to the change in spectrum. Similar slow changes in UV−visible absorption properties of the ETF FAD have been found in mutant TMADH−2ETF complexes in which Tyr-442(TMADH) has been converted to Gly-442 (*17*), suggesting that the Tyr-442 and Arg-α237 residue pair facilitates the more rapid conformational changes (<1 s) that occur in the wild-type complex (*16, 19*). In those mutant complexes where electron transfer from TMADH to ETF can be measured [e.g., TMADH(Y442G)−2ETF complexes (*16*) or TMADH−2ETF(αR237K) complexes (see below)], the difference spectral changes occur on a slower time scale than electron transfer, suggesting that these very slow changes are not relevant to the electron transfer mechanism.

Residue Networks at Domain Interfaces and Overall Structures of the Mutant ETF Proteins. Given the highly dynamic nature of ETF, major structural changes that might affect more globally the assembly of ETF with TMADH [e.g., mediated by domain III of ETF (the so-called anchor domain) or through localized unfolding of the FAD domain] is a concern. For this reason, we have solved the structures of each of the mutant ETF proteins to enable detailed structural comparison with wild-type ETF (*9*). Crystallization of mutant ETF proteins was performed following limited digestion with trypsin as described before for the wild type protein (*9*). Limited proteolysis removes the recognition loop that interacts with TMADH and allows crystallization of ETF in a high resolution diffracting space group. αR237K, αR237C, and αR237A ETF exhibited an identical digestion

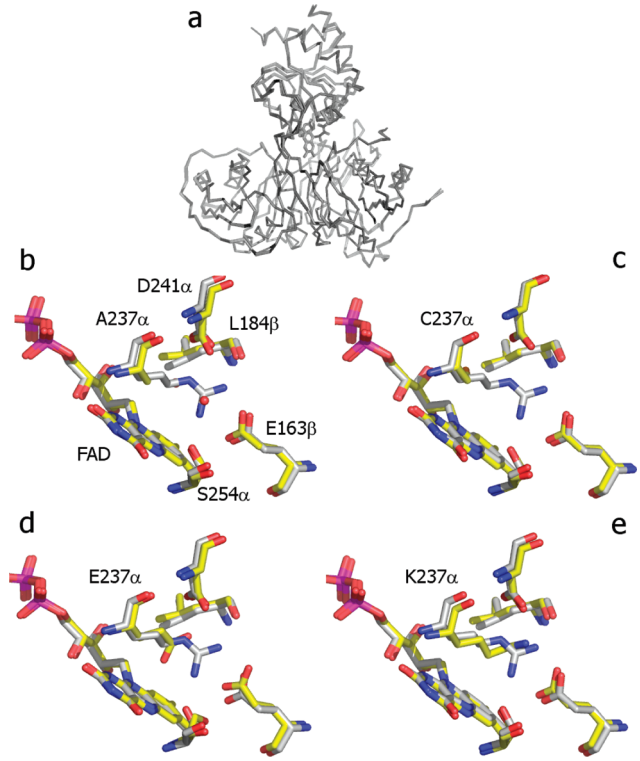

FIGURE 6: Details of the structures of the ETF mutant proteins in the vicinity of the FAD isoalloxazine ring. Panel a, ribbon representation of the structure of wild-type ETF showing domain II (the FAD-binding domain) positioned over domains I and III with the FAD isoalloxazine ring located at the domain boundaries. Panels b−d, overlay of mutant structures in the vicinity of the FAD isoalloxazine ring with the wild-type ETF structure. Panel b (mutant αR237A), panel c (mutant αR237C), panel d (mutant αR237E), and panel e (αR237K). Carbon atoms in the mutant structures are shown in yellow; carbon atoms in the wild-type structure are shown in gray. Other atoms have conventional colors.

pattern to wild-type ETF during SDS−polyacrylamide gel electrophoresis. The digestion pattern for αR237E ETF indicated the presence of an additional protein fragment of apparent molecular weight 32 kDa, suggesting a distinct conformation and/or mobility for this particular mutant in solution. Data to a resolution of 1.8, 1.65, 2.0, and 1.9 Å were used to refine the αR237K, αR237C, αR237E, and αR237A ETF structures, respectively. Data collection and structure refinement statistics are presented in Table 1. The overall structure of the αR237K ETF mutant (Figure 6) was not significantly different from that of wild-type ETF (rmsd 0.387 Å for all main chain atoms). However, the FAD-binding domain of αR237K ETF is slightly shifted compared to that of wild-type ETF as a consequence of accommodating the shorter lysine side chain. In wild-type ETF, the FAD isoalloxazine is in close contact with the Arg-α237 side chain, the latter performing a key role in establishing the domain interface. Arg-α237 forms a bifurcated salt bridge with Glu-β163, a salt linkage with Asp-α241 in addition to hydrogen bonds with Ser-α254 and the backbone of Leu-β184 (*9*). In contrast, in the αR237K ETF, Lys-α237 forms a single salt bridge with both Glu-β163 and Asp-α241 (Figure 6). Hydrogen-bonding interactions among Lys-α237, Ser-α254, and Leu-β184 were not observed in the αR237K ETF structure.

The overall structures of the αR237C and αR237A ETF were found to be identical to that of wild-type ETF (rmsd

Table 2: Average *B*-Factors for Domains I, II, and III in Wild-Type and Mutant Forms of *M. methylotrophus* ETF

average *B*-factors (Å^2)	WT	αR237A	αR237C	αR237E	αR237K
protein	27.1	21.2	26.3	20.5	31.9
α-subunit					
1−194 (domain I)	24.3	20.0	24.8	20.4	32.2
195−306 (domain II)	32.1	22.7	29.8	20.6	31.9
β-subunit					
1−236 (domain III)	25.2	20.8	24.7	20.1	31.0
237−268	38.1	26.7	37.6	25.3	37.6
overall	28.2	22.8	27.6	21.8	33.0

0.273/0.366 Å for all main chain atoms, respectively) (Figure 6). The replacement of Arg-α237 by Cys-α237 or Ala-α237 led to the loss of the key interactions described above for wild-type ETF and αR237K ETF. Moreover, water molecules could not be located in the position previously occupied by the Arg-α237 guanidinium group that could mimic its function in these mutant protein structures. In αR237C ETF, the thiol side chain does not make direct hydrogen-bonding contacts with other protein atoms, and it is stacked above the flavin ribityl group. Surprisingly, no significant conformational difference with the wild-type ETF structure could be observed for the αR237E ETF mutant, despite the different digestion pattern obtained during limited trypsin digests (rmsd 0.341 Å for all main chain atoms). The Glu-α237 side chain hydrogen bonds to Asp-α241 and is in close contact with the flavin N10. The close proximity of Glu-α237 to the flavin isoalloxazine ring has led to a reorientation of Ser-α254, breaking the hydrogen bond to the flavin N5 and establishing a hydrogen bond with Glu-*β*163. However, an extended network of direct polar contacts connecting the flavin binding domain with domains I and II as observed in the wild-type ETF and the αR237K mutant cannot be observed, although several water molecules mediate interdomain contacts.

Surprisingly, despite the obvious disruption in the network of polar contacts between the individual Arg-α237 mutant ETFs, analysis of the B-factors and TLS refinement parameters reveals the mobility of the flavin binding domain (domain II) with respect to the remainder of the structure appears significantly reduced in the individual Arg-α237 mutant structures (Table 2). The flavin binding domain (domain II) of ETF is only connected covalently to domain I via a flexible linker, but it is also associated to domain III via the C-terminal helix of the *β*-subunit which essentially behaves as part of domain II (*9*). There are very few differences within domain II in the distinct ETF crystal structures indicating that this domain is extremely compact and internally isomorphous between the different mutant crystal structures but that at the same time it is very mobile with respect to the other domains when (i) in complex with TMADH (*9*) and (ii) free in solution (*9, 14*). The average B-factor of domain II is markedly higher than that for domains I and II in the wild-type protein. This difference in average B-factor is larger for wild-type ETF compared with the corresponding values for the αR237 mutant ETFs. This might indicate that elevated mobility of this domain (compared to the rest of the structure) occurs in the wild-type protein, and assuming that the B-factors describe accurately the thermal motions at similar resolutions in the crystal structures, we conclude that the αR237 mutants represent a low vibration, locked in conformation of the molecule. Analysis of the anisotropy of domain II derived from the TLS refinement also seems to indicate a reduced structural heterogeneity in this group of mutants. We stress, however, that the crystal structures obtained provide information on only one possible conformation of the ETF proteins. The situation in solution is more complex, and a range of different conformers exist. As discussed below (see Discussion), the crystal structures obtained reveal the types of contacts that the residue at position α237(ETF) can make in one conformation, but the structures do not provide information on the relative stabilities of different conformations populated by wild-type and mutant ETF proteins. The arginine residue at position α237 is an important residue in the observed imprinting process (see below). Mutations at this position potentially restrict the conformational freedom of the molecule and similarly impair the ability of ETF to be imprinted by its redox partner. The structures reveal that Arg-α237 forms a network of interactions with residues in ETF and with TMADH (in the TMADH−2ETF complex), giving rise to a distribution of structural conformers. We suggest that mutations in this region will likely affect the dynamical properties of domain II with possible consequences for imprinting new structures of ETF through interaction with TMADH (see Discussion).

Reductive Titrations of ETF Proteins and Catalytic Reduction by TMADH. Given the overall retention of ETF structure in the mutant proteins, we hypothesized that the effects of mutating Arg-α237 should be localized to (i) the electronic properties of the FAD isoalloxazine ring and (ii) the interaction of the mobile FAD domain with TMADH, which is conjectured to be mediated through transient interaction of Tyr-442 (TMADH) with Arg-α237 (ETF) (*9*) and (iii) interaction of domain II of ETF with other ETF domains. Titration of oxidized wild-type ETF with sodium dithionite resulted in reduction of the flavin cofactor to the semiquinone (1-electron) level, but not to the hydroquinone (2-electron) level (Figure S3A), consistent with previous reports (*17*). Similarly, titration of oxidized αR237K ETF with sodium dithionite resulted in reduction of the flavin cofactor only to the semiquinone level (Figure S3B). By contrast, titration of αR237E and αR237C ETFs against sodium dithionite resulted in reduction of the FAD cofactor to the hydroquinone form (Figures S3C and D, respectively). The properties of the αR237E and αR237C ETFs mirror our previous observations with αR237A ETF (*17*).

Spectral analysis of the reduction of each ETF protein was extended to include reduction by the physiological partner TMADH. Reduction of oxidized wild-type ETF by catalytic amounts of TMA-reduced TMADH produced the semiquinone form of the protein and not the hydroquinone form, despite prolonged incubation with the reducing system (Figure 7A). The spectral changes are consistent with those reported by others (*3, 17*). The spectral changes are similar to those generated on titration of wild-type ETF with sodium dithionite (Figure S3A). Reduction of oxidized αR237K ETF by catalytic amounts of TMA-reduced TMADH also generated the semiquinone form of the protein (Figure 7B). Oxidized αR237A ETF was reduced by TMADH to the hydroquinone form of the protein within ~24 h under the conditions used, but full reduction of oxidized αR237C and αR237E ETF was not complete within 48 h (Figure 7C and

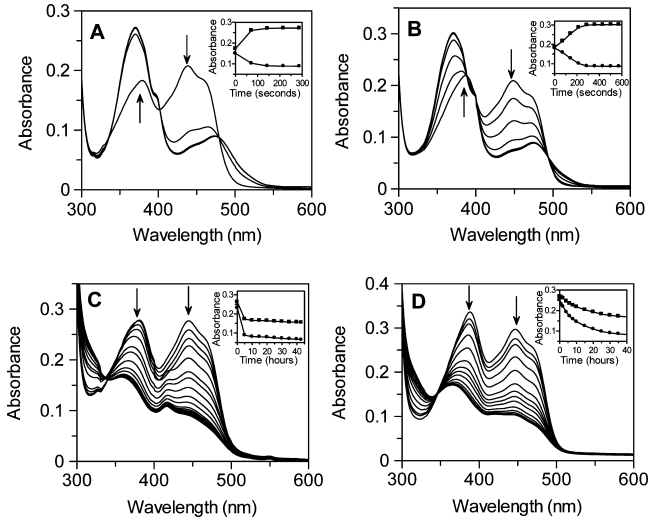

FIGURE 7: Absorbance changes accompanying reductive titrations of wild-type and mutant ETF proteins by catalytic amounts of TMA-reduced TMADH. Panel A: titration of wild-type ETF_{ox}. Panel B: titration of αR237K ETF_{ox}. Panel C: titration of the αR237C ETF_{ox}. Panel D: titration of αR237E ETF_{ox}. Conditions: TMADH (0.1 μM reduced with 10 mM TMA) and 50 mM potassium phosphate buffer at pH 7.0 and 25 °C. Assays were performed under strict anaerobic conditions.

D, respectively) despite the concentration of TMADH being increased 10-fold over that used for the reduction of wild-type ETF.

The assays described above were extended to obtain Michaelis parameters for steady-state reduction of ETF by TMADH. A plot of the rate of ETF reduction versus αR237K ETF concentration was fitted to the Michaelis−Menten equation yielding a K_m of 3.1 ± 0.3 μM (10.5 ± 0.69 μM for wild-type ETF) and a turnover rate constant of 1.46 ± 0.04 s^{-1} (9.67 ± 0.17 s^{-1} for wild-type ETF). Significant reduction by TMADH of oxidized αR237C, αR237E, and αR237A ETF was not observed over 15 min, thus preventing determination of kinetic constants under aerobic and anaerobic conditions. The data indicate substantial impairment in electron transfer activity in these mutant electron transfer complexes. We infer that the substantially impaired ability of TMADH to reduce the αR237A, αR237C, and αR237E ETFs is related to the removal of Arg-α237, which either (i) prevents transient stabilization of the FAD-binding domain in the electron transfer competent state, which is likely stabilized in the wild-type complex through interaction of Arg-α237 with Tyr-442 (TMADH), and/or (ii) perturbs the redox potential of the FAD in ETF so as to make electron transfer unfavorable from TMADH (see below). That substantial activity is retained in the complex formed with αR237K ETF suggests that the positively charged lysine side chain is able to engage in an interaction with Tyr-442 to form an electron transfer competent state during the conformational sampling mechanism and that any altered potential for the FAD cofactor in the αR237K ETF is not sufficiently large so as to adversely effect electron transfer. To ascertain the effects of mutation on the potentials of the FAD cofactor in the mutant ETFs we have performed potentiometry studies of each form (described below).

Potentiometric Titrations of ETF Proteins. We have previously determined the midpoint potentials for wild-type ETF and the αR237A mutant [(*17*); Table 3]. The FAD

Table 3: Midpoint Reduction Potentials for Wild-Type and αR237 Mutants of ETF[a]

ETF	midpoint potential of E_1' couple (mV)	midpoint potential of E_2' couple (mV)
wild-type[b]	+153 ± 2	<−250
αR237A[b]	−43 ± 2	−31 ± 2
αR237K	+62 ± 2	<−250
αR237C	−57 ± 4	−145 ± 5
αR237E	−59 ± 2	−199 ± 2

[a] Values were determined from the fit to eq 1. E_1' and E_2' are the midpoint potential for oxidized/semiquinone and semiquinone/reduced couples, respectively. [b] Taken from ref *17*.

reduction potential of the oxidized-semiquinone couple in the wild-type is +153 ± 2 mV, indicating exceptional stabilization of the flavin anionic semiquinone species. Conversion to the dihydroquinone is incomplete because of the presence of both kinetic and thermodynamic blocks on full reduction of the FAD. The crystallographic structure of ETF suggests that the guanidinium group of Arg-α237, which is located over the *si*-face of the flavin isoalloxazine ring, plays a key role in this exceptional stabilization of the anionic semiquinone in wild-type ETF (*9*). Mutation of Arg-α237 to alanine resulted in a remarkable ∼200 mV destabilization of the flavin anionic semiquinone (*17*). In addition, reduction to the hydroquinone in the αR237A ETF is relatively facile; this indicates that the kinetic block seen in wild-type ETF is substantially removed in the αR237A ETF (*17*). The mutation of Arg-α237 to Ala-α237 represents a substantive change in side chain structure, thus potentiometric analysis of the other mutant ETFs, particularly in light of the crystal structures reported above, is informative. We have thus extended these potentiometric studies to the αR237K, αR237C, and αR237E to assess the impact of the mutations on the thermodynamic properties of the FAD (Figure S4; Table 3). In these studies, oxidized αR237K ETF was reduced to the semiquinone form. A plot of absorbance at 370 and 470 nm versus potential was fitted to the appropriate Nernst function and the ETF_{ox}/ETF_{sq} couple calculated as +62 ± 5 mV. The ETF_{sq}/ETF_{hq} couple remained <−250 mV [as for wild-type ETF (*17*)]. Thus, mutation of αArg-237 to lysine destabilizes the semiquinone species by ∼90 mV. Oxidized αR237C ETF was reduced to the hydroquinone form via the 1-electron reduced semiquinone state. The ETF_{ox}/ETF_{sq} couple was calculated as −57 ± 4 mV and the ETF_{sq}/ETF_{hq} couple as −145 ± 5 mV. Similarly, both couples were evident in titration of αR237E ETF with dithionite (ETF_{ox}/ETF_{sq} as −59 ± 5 mV; ETF_{sq}/ETF_{hq} couple as −199 ± 2 mV). The oxidized/semiquinone FAD couple is therefore substantially destabilized (by ∼210 mV and ∼212 mV) in the αR237C and αR237E ETFs, respectively. This in part probably accounts for the very slow and incomplete reduction of these ETF proteins by TMADH given that the midpoint reduction potential of the 4Fe-4S center has been reported as being ∼100 mV (*27*). These data indicate that Arg-α237 has an important role in stabilizing the semiquinone form of ETF, which is an important aspect of the electron transfer mechanism. This is in addition to its proposed role in transiently stabilizing the FAD domain through interaction with Tyr-442 (TMADH) during the conformational search for productive electron transfer configurations (*9*).

Probing the Involvement of Arg-α237 in Structural Imprinting of ETF by TMADH. Attempts to imprint the αR237 ETF mutants by TMADH were performed as described for wild-type ETF. As with wild-type complex studies, fluorescence changes as a function of time were not observed for either TMADH or ETF in the absence of the interacting partner protein. Owing to the different redox stabilities of the mutant ETF proteins, only the as-purified αR237K and dithionite-titrated αR237E ETFs[3] were studied in the semiquinone state. In these cases, no significant change in fluorescence or absorbance (from which imprinting of ETF is inferred) was observed on reaction of these αR237 mutant ETFs with TMADH over a minimum period of 3 h. The absence of any significant fluorescence and spectral changes suggests that Arg-α237 is required to elicit the fluorescence change associated with imprinting, consistent with the structural change being localized close to the FAD isoalloxazine ring. The oxidized forms of the αR237C and αR237E ETFs did not give rise to fluorescence changes or spectral perturbation in imprinting assays. This is consistent with data obtained for oxidized wild-type ETF. On the basis of these data and observations made with wild-type ETF, we have proposed a minimal structural model for the imprinting phenomenon (see Discussion).

EPR saturation profiles for the semiquinone forms of the mutant ETFs compared with wild-type ETF are presented in Supporting Information (Figures S5A−E). The Co^{2+} relaxation data are qualitatively similar to data collected for as-purified wild-type ETF, suggesting that the FAD is solvent exposed, as would be expected from the crystal structures of the proteins. The degree of microwave saturation seen for each mutant suggests some differences in the extent of FAD motion in the mutant proteins. Additionally, the effects of Co^{2+} ion addition suggest different degrees of solvent accessibility to the FAD. Although these studies are useful in suggesting different dynamic properties for the ETF proteins and altered degrees of solvent exposure of the FAD and/or access of the Co^{2+} ion to the FAD center, it is not possible to rigorously quantify these effects in relation to the solution structure and dynamics of the various ETF proteins.

DISCUSSION

The Phenomenon of Structural Imprinting. There has been some confusion in the literature about the existence of an imprinting phenomenon in *M. methylotrophus* ETF (*18, 29*). Using fluorescence of the FAD as a probe, we had previously reported that as-purified ETF undergoes a slow conformational change on incubation with TMADH and that the rate of this conformational change is relatively slow (i.e., much slower than the rate of electron transfer between TMADH and ETF). It is important not to confuse structural imprinting with the mechanism of conformational sampling that we advanced as a result of our crystallographic studies of the TMADH−2ETF complex (*9*). The existence of the imprinting phenomenon has been questioned recently (*28*), but we have now clarified this situation and offer below potential explanations for this apparent disparity.

First, we have extended our imprinting studies to include analysis of as-purified and imprinted wild-type ETF using EPR spectroscopy. Our EPR data (Figures 4) corroborate our earlier findings inferred from fluorescence analysis that as-purified ETF does undergo a slow structural change on incubation with TMADH. We have demonstrated that this change is not redox linked (TMADH is fully oxidized prior to addition to as-purified ETF) and does not involve molecular oxygen (imprinting occurs under strictly anaerobic conditions). Moreover, imprinting is not the result of FAD modification (Figure 3). We have shown that imprinted ETF is relatively stable since removal of TMADH (through exploitation of the engineered His tag on TMADH) after the imprinting reaction does not alter the final conformational state of ETF. Furthermore, this demonstrates that the structurally altered form of ETF is not restricted to ETF in complex with TMADH, but also occurs in uncomplexed ETF. We have shown that imprinting is restricted to the as-purified form of ETF_{sq} since redox cycling (oxidation followed by reduction using ferricyanide and dithionite, respectively) generates a semiquinone form of ETF that is not imprinted by TMADH. Moreover, the fluorescence properties of the FAD in ETF_{ox} are not perturbed on addition of TMADH. Thus, imprinting is a peculiar property of the semiquinone form of the protein present in the as-purified form of ETF. An explanation for the apparent discrepancy between our own observations and those of Hille and coworkers who did not observe imprinting in ETF is, as far as we can infer from published data (*28*), related to the method used to prepare ETF_{sq}. If ETF is redox cycled to generate ETF_{sq}, it is clear from our own studies that ETF_{sq} will not imprint. Notwithstanding, it is also clear from our studies reported in this article that as-purified ETF_{sq} *does* undergo a slow structural change following interaction with TMADH, that is, the imprinting reaction. Thus, our work emphasizes the need for caution in comparing the biophysical properties of highly dynamic redox proteins [e.g., ETFs (*10*−*13*), nitric oxide synthases (*29*), and similar dynamic proteins] reported from different laboratories. This follows owing to potential differences in behavior and the conformational states obtained, which are attributed to different methods of preparing the proteins.

The additional analysis of imprinting we have reported in this article is entirely consistent with our previous studies of as-purified ETF_{sq} (*18*). Previously, we demonstrated that imprinted ETF_{sq} reacted more rapidly than as-purified ETF with exogenous electron acceptors such as the ferricenium ion (*18*). We inferred that there was improved solvent access to the FAD in imprinted ETF, a suggestion that is now supported by the EPR studies reported in this article. We wish to point out, however, that our previous study with oxidized ETF indicated a smaller increase in FAD fluorescence on incubation with TMADH. In our more extensive analysis described in this article, we were unable to show this phenomenon with ETF_{ox} that had been generated by chemical treatment with ferricyanide. It is long established in the ETF literature that ETF_{ox} is relatively unstable, and we suggest the relatively small fluorescence changes (com-

[3] That the αR237E ETF is purified in the oxidized form and needs to be reduced through chemical reduction prior to imprinting analysis is a potential concern. This is because of the inability of oxidized wild-type ETF to become imprinted on interaction with TMADH. Consequently, we place more prominence on the αR237K ETF data (which is purified in the semiquinone state) in pointing to the importance of residue Arg-α237 in the imprinting process.

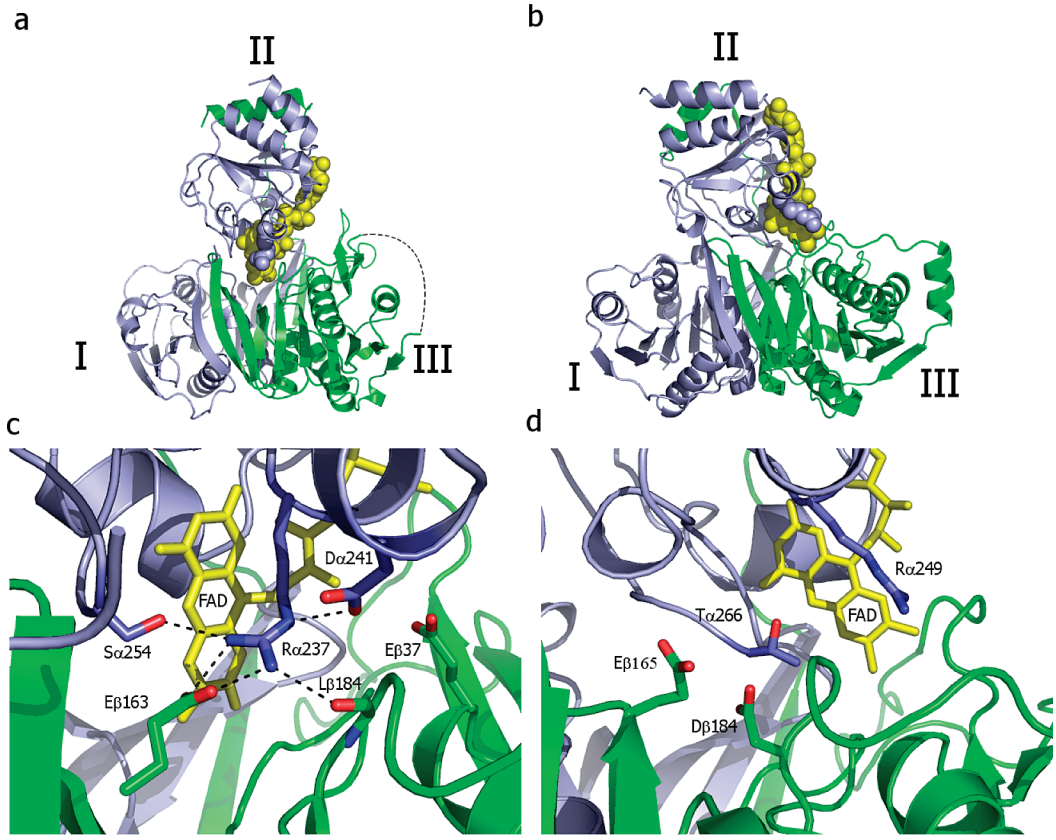

FIGURE 8: Comparison of domain II orientation in the crystal structures of *M. methylotrophus* ETF and human ETF. The α subunit is shown in blue and the *β* subunit in green. Panel a, relative domain organisation in the crystal structure of *M. methylotrophus* ETF. The hatched region indicates the location of the recognition loop for interaction with TMADH, which is excised by limited proteolysis to favor crystallization of ETF. Panel b, relative domain organization in the crystal structure of human ETF. Panels c and d, structural detail close to the FAD isoalloxazine ring illustrating the closed nature and residue interactions of Arg-α237 with neighboring residues in *M. methylotrophus* ETF and the relatively open nature of the corresponding region in human ETF. Comparison of the structures suggests that *M. methylotrophus* ETF (and human ETF) might sample a number of conformations, some akin to those found in the crystal structures of *M. methylotrophus* and human ETF, thus accounting for the expanded envelope seen for domain II in SAXS studies with both proteins (*14*). We suggest that the ability of Arg-α237 to interact with different residues in ETF and Tyr-442 (TMADH) to generate altered conformations of ETF also accounts for the imprinting of wild-type ETF by TMADH, although the precise structural changes remain to be elucidated.

pared with imprinting reactions for as-purified ETF_{sq}) that we observed in our previous study might represent some loss of FAD from oxidized ETF. It is clear from our current work that imprinting of ETF_{sq} cannot be attributed to loss of FAD_{sq} (as this would be rapidly oxidized), and our EPR and UV−visible studies clearly indicated that imprinted ETF contains bound FAD_{sq}.

A Minimal Model for Structural Imprinting. We have demonstrated that Arg-α237 is an important determinant of the imprinting phenomenon since mutants altered at this position do not show altered fluorescence properties on incubation with TMADH. This finding mirrors our previous report with mutant forms of TMADH altered at residue Tyr-442 (*18*). In light of the crystal structure of the TMADH−2ETF complex (*9*), these data suggest that interaction of ETF domain II with TMADH through Tyr-442 (TMADH) and Arg-α237 (ETF) is important in eliciting a conformational change in as-purified ETF_{sq}. Given the dynamic nature of ETF, we infer that as-purified ETF_{sq} is purified in a distinct structural state and that interaction with TMADH leads to a change in conformation mediated by the Tyr-442 (TMADH) and Arg-α237 (ETF) interaction. The crystal structure of as-purified *M. methylotrophus* ETF reveals that domain II occupies a conformation different from that observed in the structure of human ETF (Figure 8). In *M. methylotrophus* ETF, the FAD isoalloxazine ring is relatively more buried compared with the situation in human ETF, and in this closed conformation, the guanidinium group of Arg-α237 interacts with Glu-*β*163 and other neighboring residues (Figure 8a and c). Our previous modeling of the TMADH−2ETF complex (*9*) indicates that this network of interactions is broken on addition of TMADH to allow the transient interaction of Arg-α237 (ETF) with Tyr-442 (TMADH). This occurs because the structure of free *M. methylotrophus* ETF must adopt a more human-like conformation to enable its interaction with TMADH (*9*). This therefore brings about a change in the conformation of domain II of *M. methylotrophus* ETF so that on dissociating from TMADH it would adopt a position more similar to that seen in the crystal structure of human ETF (Figure 8b). In this more open (human) conformation, Arg-α237 is ideally positioned to interact with Glu-*β*37, thus stabilizing this open conformation when ETF dissociates from TMADH. The slow kinetics of imprinting indicate a relatively large barrier, which no doubt reflects the disruption of a number of interactions made by Arg-α237 in the more closed conformation of as-purified ETF_{sq} (Figure 8c).

Conversion to a more open human-like state on interaction of as-purified ETF with TMADH is consistent with our EPR studies that suggest that the FAD is more exposed to solvent

in the imprinted form of wild-type ETF (Figure 4). In oxidized ETF, the stability of the buried conformation might be compromised, accounting for the apparent lack of imprinting of ETF following flavin oxidation. In the mutant ETF proteins, the stability of the closed conformation is also likely to be compromised owing to disruption of interactions made by Arg-α237 in the more closed conformation of wild-type ETF. There may, of course, be other conformational states of ETF, not yet identified. Our minimal structural model is based on available experimental data, which is consistent with the perceived role of Arg-α237 in perturbing the conformational distribution through interaction with Tyr-442, thus providing a rationale for the lack of imprinting activity with the mutant forms of ETF.

That the wild-type and mutant forms of ETF were crystallized in a similar conformational state (essentially a closed conformational state) indicates that the mutant forms are able to populate to some degree the closed state (although these states are likely to be less stable in the mutant proteins owing to disruption of the interactions shown in Figure 8c following mutagenesis). We have made repeated attempts to crystallize the imprinted, open form of wild-type ETF_{sq} and also oxidized wild-type ETF, but this has been without success. Our crystallization conditions apparently select for a closed conformation. It is important to emphasize that, although structures were obtained for the mutant forms in the closed conformation, this says little about the relative stabilities of the open and closed conformations in wild-type and mutant forms of ETF. Consequently, one should not use this as a guide to the relative stabilities of different conformational states in solution.

Multiple Roles for Arg-α237 in the TMADH−2ETF Complex. The slow structural imprinting phenomenon observed for as-purified ETF_{sq} is unlikely to impact the physiological mechanism of electron transfer, but the structural model does serve to emphasize the dynamic properties of ETF and the potential to populate different conformational states in which Arg-α237 can make a number of different interactions. On the basis of modeling studies, we have suggested previously that conformational sampling [which is an integral part of the electron transfer mechanism (*9*)] must occur from a series of more open conformations of ETF [i.e., similar to the structure of human ETF (Figure 8b)]. When in complex with TMADH, the more open conformations of domain II will enable Arg-α237 to interact with a number of potential partners [e.g., Glu-*β*37 (ETF) and Tyr-442 (TMADH)]. Our model for productive electron transfer invokes a transient freezing of the motion of domain II in the conformational sampling mechanism by interaction with Tyr-442 (TMADH). This brings the electron transfer distance from the TMADH 4Fe-4S center to the ETF FAD comfortably within the 14 Å window required to support a physiologically relevant rate of interprotein electron transfer. Such a model is consistent with the very poor rates of electron transfer we have observed with the αR237A/C/E mutants. That electron transfer is only affected to a small extent with the αR237K ETF implies that residue Lys-α237 can to some extent mimic the role of Arg-α237 in the wild-type TMADH−2ETF complex.

We have also demonstrated that mutation of Arg-α237 leads to substantial perturbation of the redox potential of the FAD bound to ETF. The midpoint reduction potential of the 4Fe-4S center in TMADH has been reported as being +102 mV (*27*). That the oxidized/semiquinone redox couple in wild-type ETF is +153 mV (*17*) is consistent with the need to transfer an electron to ETF. Mutation of Arg-α237, however, leads to substantial destabilization of the oxidized/semiquinone couple such that electron transfer to the mutant ETF proteins is endergonic (Table 3). Destabilization is least in the αR237K mutant, and consequently, electron transfer is not adversely affected in this mutant TMADH−2ETF complex, but the extent of perturbation of the potentials in the remaining mutant proteins is so large that these likely account for the very slow rate of electron transfer measured in turnover assays with these ETF mutant proteins.

The proposed central role of the Tyr-442 and Arg-α237 interaction in transiently stabilizing an electron transfer competent conformation is consistent with our previous kinetic study of mutant complexes in which Tyr-442 was targeted for mutagenesis. In this study, conformational sampling becomes rate limiting following mutagenesis of Tyr-442, probably through an impaired ability to transiently freeze the motion of domain II in an electron transfer competent configuration (*16*). In stopped-flow studies of electron transfer in the wild-type complex, we have shown that the rate of electron transfer is linearly dependent on ETF concentration, whereas in mutant complexes altered at residue 442, the rate dependence becomes hyperbolic on ETF concentration (*16*). This switch in response to ETF concentration is consistent with the mutant Y442F, Y442S, and Y442G complexes being less able to stabilize a productive electron transfer configuration during the conformational sampling mechanism as a result of engineering out the key Tyr-442−Arg-α237 interacting pair. Such a kinetic response demonstrates another key role for Arg-α237 in the conformational sampling mechanism. This is in addition to its important roles in (i) poising the potential of the FAD cofactor and (ii) controlling the dynamical nature of ETF through its interaction with neighboring residues in ETF.

Concluding Remarks. Arg-α237 has multiple and important roles in the TMADH−2ETF complex and interprotein electron transfer. The residue stabilizes the oxidized/semiquinone couple of the ETF FAD to allow productive electron transfer from the 4Fe-4S center of TMADH. The residue has multiple interacting partners that enable ETF to explore a number of different conformational states in solution. We have also shown that Arg-α237 is implicated in structural imprinting of ETF, and we have clarified the apparent discrepancy in the literature relating to this phenomenon. Our previous (*9, 16*) and current studies support a mechanism in which interaction of Arg-α237(ETF) with Tyr-442 (TMADH) transiently stabilizes an electron transfer competent conformation of the TMADH−2ETF complex. Our analysis is consistent with a complex mechanism of electron transfer invoking initial binding of the partner proteins, conformational sampling, and electron exchange, the concept of which might translate to other dynamically coupled electron transfer systems in biology.

SUPPORTING INFORMATION AVAILABLE

Fluorescence data (molecular imprinting control reactions), absorbance data (complex formation and potentiometry), and EPR data (microwave saturation profiles for mutant ETF

proteins). This material is available free of charge via the Internet at http://pubs.acs.org.

REFERENCES

1. Thorpe, C. (1991) Electron Transferring Flavoproteins, in *Chemistry and Biochemistry of Flavoenzymes* (Muller, F.) Vol. II, pp 471−486, CRC Press, Boca Raton, FL.
2. Husain, M., and Steenkamp, D. J. (1985) Partial purification and characterization of glutaryl-coenzyme A dehydrogenase, electron transfer flavoprotein, and electron transfer flavoprotein-Q oxidoreductase from *Paracoccus denitrificans*. *J. Bacteriol. 163*, 709–715.
3. Steenkamp, D. J., and Gallup, M. (1978) The natural flavoprotein electron acceptor of trimethylamine dehydrogenase. *J. Biol. Chem. 253*, 4086–4089.
4. Eichler, K., Buchet, A., Bourgis, F., Kleber, H. P., and Mandred-Berthelot, M. A. (1995) The fix *Escherichia coli* region contains four genes related to carnitine metabolism. *J. Basic Microbiol. 35*, 217–227.
5. Tsai, M. H., Jr. (1995) Phylogenetic characterization of the ubiquitous electron transfer flavoprotein families ETF-alpha and ETF-beta. *Res. Microbiol. 146*, 397–404.
6. Earl, C. D., Ronson, C. W., and Ausubel, F. M. (1987) Genetic and structural analysis of the Rhizobium meliloti fixA, fixB, fixC, and fixX genes. *J. Bacteriol. 169*, 1127–1136.
7. Whitfield, C. D., and Mayhew, S. G. (1974) Purification and properties of electron-transferring flavoprotein from *Peptostreptococcus elsdenii*. *J. Biol. Chem. 249*, 2801–2810.
8. Scrutton, N. S., and Sutcliffe, M. J. (2000) Trimethylamine dehydrogenase and electron transferring flavoprotein. *Subcell. Biochem. 35*, 145–181.
9. Leys, D., Basran, J., Sutcliffe, M. J., and Scrutton, N. S. (2003) Extensive conformational sampling in a ternary electron transfer complex. *Nat. Struct. Biol. 10*, 219–225.
10. Leys, D., and Scrutton, N. S. (2004) Electrical circuitry in biology: emerging principles from protein structure. *Curr. Opin. Struct. Biol. 14*, 1–14.
11. Toogood, H. S., van Thiel, A., Basran, J., Sutcliffe, M. J., Scrutton, N. S., and Leys, D. (2004) Extensive domain motion and electron transfer in the human electron transferring flavoprotein·medium chain Acyl-CoA dehydrogenase complex. *J. Biol. Chem. 279*, 32904–32912.
12. Toogood, H. S., van Thiel, A., Scrutton, N. S., and Leys, D. (2005) Stabilization of non-productive conformations underpins rapid electron transfer to electron-transferring flavoprotein. *J. Biol. Chem. 280*, 30361–30366.
13. Toogood, H. S., Leys, D., and Scrutton, N. S. (2007) Dynamics driving function − new insights from electron transferring flavoproteins and partner complexes. *FEBS J. 274*, 5481–5504.
14. Jones, M., Basran, J., Sutcliffe, M. J., Grossmann, J. G., and Scrutton, N. S. (2000) X-ray scattering studies of Methylophilus methylotrophus (sp. W3A1) electron-transferring flavoprotein. Evidence for multiple conformational states and an induced fit mechanism for assembly with trimethylamine dehydrogenase. *J. Biol. Chem. 275*, 21349–21354.
15. Chohan, K. K., Jones, M., Grossmann, J. G., Frerman, F. E., Scrutton, N. S., and Sutcliffe, M. J. (2001) Protein dynamics enhance electronic coupling in electron transfer complexes. *J. Biol. Chem. 276*, 34142–34147.
16. Basran, J., Chohan, K. K., Sutcliffe, M. J., and Scrutton, N. S. (2000) Differential coupling through Val-344 and Tyr-442 of trimethylamine dehydrogenase in electron transfer reactions with ferricenium ions and electron transferring flavoprotein. *Biochemistry 39*, 9188–9200.
17. Talfournier, F., Munro, A. W., Basran, J., Sutcliffe, M. J., Daff, S., Chapman, S. K., and Scrutton, N. S. (2001) αArg-237 in Methylophilus methylotrophus (sp. W3A1) electron transferring flavoprotein affords ∼200 mV stabilization of the FAD anionic semiquinone and a kinetic block on full reduction to the dihydroquinone. *J. Biol. Chem. 276*, 20190–20196.
18. Jones, M., Talfournier, F., Bobrov, A., Grossmann, J. G., Vekshin, N., Sutcliffe, M. J., and Scrutton, N. S. (2002) Electron transfer and conformational change in complexes of trimethylamine dehydrogenase and electron transferring flavoprotein. *J. Biol. Chem. 277*, 8457–8465.
19. Jang, M. H., Scrutton, N. S., and Hille, R. (2000) Formation of W3A1 electron-transferring flavoprotein (ETF) hydroquinone in the trimethylamine dehydrogenase−ETF protein complex. *J. Biol. Chem. 275*, 12546–12552.
20. Steenkamp, D. J., and Mallinson, J. (1976) Trimethylamine dehydrogenase from a methylotrophic bacterium I. Isolation and steady-state kinetics. *Biochim. Biophys. Acta 429*, 705–719.
21. Scrutton, N. S., Packman, L. C., Mathews, F. S., Rohlfs, R. S., and Hille, R. (1994) Assembly of redox centers in the trimethylamine dehydrogenase of bacterium W3A1. Properties of the wild-type enzyme and a C30A mutant expressed from a cloned gene in *E. coli*. *J. Biol. Chem. 269*, 13942–13950.
22. Wilson, E. K., Huang, L. X., Sutcliffe, M. J., Mathews, F. S., Hille, R., and Scrutton, N. S. (1997) An exposed tyrosine on the surface of trimethylamine dehydrogenase facilitates electron transfer to electron transferring flavoprotein: kinetics of transfer in wild-type and mutant complexes. *Biochemistry 36*, 41–48.
23. Dutton, P. L. (1978) Redox potentiometry: determination of midpoint potentials of oxidation-reduction components of biological electron-transfer systems. *Methods Enzymol. 54*, 422–435.
24. Otwinowski, Z., and Minor, W. (1997) Processing of X-ray diffraction data collected in oscillation mode. *Methods Enzymol. 276*, 307–326.
25. Murshudov, G. N., Vagin, A. A., and Dodson, E. J. (1997) Refinement of macromolecular structures by the maximum-likelihood method. *Acta Crystallogr., Sect. D 53*, 240–255.
26. Perrakis, A., Harkiolaki, M., Wilson, K. S., and Lamzin, V. S. (2001) ARP/wARP and molecular replacement. *Acta Cryst., Sect. D 57*, 1445–1450.
27. Barber, M. J., Pollock, V., and Spence, J. T. (1988) Microcoulometric analysis of trimethylamine dehydrogenase. *Biochem. J. 256*, 657–659.
28. Shi, W., Mersfelder, J., and Hille, R. (2005) The interaction of trimethylamine dehydrogenase and electron transferring flavoprotein. *J. Biol. Chem. 280*, 20239–20246.
29. Dunford, A. J., Rigby, S. E., Hay, S., Munro, A. W., and Scrutton, N. S. (2007) Conformational and thermodynamic control of electron transfer in neuronal nitric oxide synthase. *Biochemistry 46*, 5018–5029.

BI800127D